Annealing-induced enhancement of ferromagnetism and nanoparticle formation in the ferromagnetic semiconductor GeFe

Yuki K. Wakabayashi, Yoshisuke Ban, Shinobu Ohya, and Masaaki Tanaka
Department of Electrical Engineering and Information Systems, The University of Tokyo, 7-3-1 Hongo, Bunkyo-ku, Tokyo 113-8656, Japan
(Received 22 April 2014; published 14 November 2014)

We report the annealing-induced enhancement of ferromagnetism and nanoparticle formation in group-IV-based ferromagnetic semiconductor GeFe. We successfully increase the Curie temperature of the $Ge_{0.895}Fe_{0.105}$ film up to 210 K while keeping a nearly single ferromagnetic phase when the annealing temperature is lower than 600 °C. In contrast, when it is annealed at 600 °C, single-crystal GeFe nanoparticles with stacking faults and twins, which have high Curie temperature up to room temperature, are formed in the film. We show that the inhomogeneity of the Fe concentration plays an essential role in determining the ferromagnetism in both cases. Although all the GeFe films show weak spin-glass-like behavior in the very low-temperature region (lower than ∼26 K), which is insensitive to the annealing temperature, due to the nonuniform distribution of the Fe atoms, the ferromagnetism is much stronger than the spin glass and it dominates the system.

DOI: 10.1103/PhysRevB.90.205209 PACS number(s): 75.70.Ak, 75.50.Pp, 68.55.−a

I. INTRODUCTION

The ferromagnetic materials based on group-IV-semiconductor Ge, including Ge-based ferromagnetic semiconductors (FMSs) and ferromagnetic nanoparticles embedded in Ge, are very promising for future Si-based spintronic devices. Among them, GeMn and GeFe have been intensively studied, since these materials have some advantages; they can be epitaxially grown on Si substrates [1,2], flat and smooth interfaces with Si without a disordered interfacial layer can be formed, and there is no conductivity mismatch problem with Si. Therefore they will be efficient spin injectors and detectors where the spin-flip scattering at the interfaces is suppressed. Many studies have been carried out on Mn-doped Ge($Ge_{1-x}Mn_x$) films [3–6], and they frequently have ferromagnetic intermetallic precipitates such as Mn_5Ge_3, $Mn_{11}Ge_8$ [5] or amorphous $Ge_{1-x}Mn_x$ [6]. In the case of $Ge_{1-x}Fe_x$ films, we can grow single-crystal films of a diamond type with a nonuniform distribution of Fe atoms without any intermetallic Fe-Ge compounds, and we can control the conductivity by boron (B) doping independently of the Fe concentration x [7]. These features are appropriate for spin-injection applications; however, the current problem of GeFe is its low Curie temperature (T_C), which is at the highest 170 K so far [8–10]. Recently, GeFe quantum dots with a high T_C of ∼400 K without any observable precipitates have been reported [11]. Thus, if we can grow GeFe quantum dots (or nanoparticles) inside a Ge film with a flat surface or interfaces with other layers (or substrates), they are very promising. In fact, the ferromagnetic MnAs nanoparticles embedded in GaAs have shown intriguing properties induced by Coulomb blockade and spin-dependent tunneling [12,13]. In III-V-based FMS (Ga,Mn)As, post-growth annealing is known to be a powerful technique to improve the T_C by removing the interstitial Mn atoms from the (Ga,Mn)As layer [14,15]. Here, we investigate the annealing effect on GeFe in order to enhance the ferromagnetism of GeFe and its relevance to the structural and magnetic properties. Through this study, we find that the evolution mechanism of the ferromagnetism of GeFe is largely different from that of the conventional III-V-based FMSs GaMnAs and InMnAs, and even from that of the group-IV-based FMS GeMn.

II. GROWTH

The $Ge_{0.895}Fe_{0.105}$ thin film studied here was epitaxially grown on a Ge(001) substrate by low-temperature molecular beam epitaxy (LT-MBE). The growth process is described as follows. After the Ge(001) substrate was chemically cleaned and its surface was hydrogen-terminated by buffered HF solution, it was introduced in the MBE growth chamber through an oil-free load-lock system. After degassing the substrate at 400 °C for 30 min and successive thermal cleaning at 900 °C for 15 min, a 30-nm-thick Ge buffer layer was grown at 200 °C, followed by the growth of a 60-nm-thick $Ge_{0.895}Fe_{0.105}$ layer at 240 °C. The *in situ* reflection high-energy electron diffraction (RHEED) was used to observe the crystallinity and morphology of the surface during the growth. The diffraction pattern of the Ge buffer layer surface showed intense and sharp 2×2 streaks, and the $Ge_{0.895}Fe_{0.105}$ surface also showed a 2×2 pattern with no extra spots, indicating two-dimensional epitaxial growth. Post-growth annealing was carried out in a nitrogen atmosphere for 30 min at 400, 500, and 600 °C.

III. CRYSTALLOGRAPHIC ANALYSES

The crystallographic analyses of the $Ge_{0.895}Fe_{0.105}$ films were performed by high-resolution transmission-electron microscopy (HRTEM). Figures 1(a) and 1(b) show the HRTEM lattice images of the $Ge_{0.895}Fe_{0.105}$ film as-grown and annealed at 500 °C projected along the Ge [110] axis, respectively. Both images indicate that the $Ge_{0.895}Fe_{0.105}$ layers have a diamond-type single-crystal structure with an atomically flat surface. Although the color (dark and bright) contrast in the GeFe layer is attributed to the nonuniform distribution of Fe atoms and stacking-fault defects as discussed in Ref. [10], there are no other ferromagnetic intermetallic Fe-Ge precipitates with a different crystal structure.

Figure 1(c) shows a HRTEM lattice image of the $Ge_{0.895}Fe_{0.105}$ film annealed at 600 °C projected along the Ge [110] axis, where we see many nanoparticles formed in the film. Figure 2(a) shows the magnified view of the HRTEM lattice image of one of the nanoparticles in the $Ge_{0.895}Fe_{0.105}$ film annealed at 600 °C, indicating that the nanoparticles

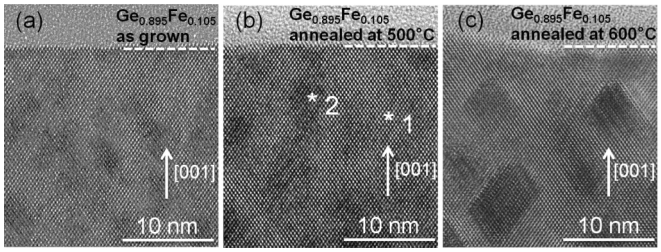

FIG. 1. HRTEM lattice images projected along the Ge[110] axis of $Ge_{0.895}Fe_{0.105}$ (a) as-grown and after annealing at (b) 500 °C and (c) 600 °C.

have periodic twins and stacking faults. By the spatially resolved transmission electron diffraction (TED) combined with the energy-dispersive x-ray spectroscopy (EDX), the local electron-diffraction pattern and the local Fe concentration were obtained. In the EDX measurements, the error bar of the Fe concentration is ±1%, which mainly originates from the sample drift of ∼1 nm during the measurements. The local Fe concentration at *1 (bright region) and *2 (dark region) of the GeFe film annealed at 500 °C shown in Fig. 1(b) was estimated to be 8% and 23%, respectively. When the annealing temperature is 600 °C, the local Fe concentration at *1 (homogeneous diamond-crystal-structure region) and *2 (inside the nanoparticle) in Fig. 2(a) was estimated to be 5% and 25%, respectively. These results indicate that the higher the annealing temperature is, the larger the nonuniformity of the Fe concentration becomes. Figure 2(b) shows the TED image at *1, exhibiting the diffraction pattern of the diamond-type lattice structure with extremely weak extra spots due to stacking-fault defects. Figure 2(c) shows the TED image at *2, indicating a similar diffraction pattern of the diamond-type lattice structure including clear twins and stacking faults [16]. In either TED images, we do not see any diffractions from precipitates with crystalline Fe-Ge intermetallic compounds of other crystal structures.

IV. MAGNETIC PROPERTIES

Magneto-optical measurements were performed in order to investigate the magnetic properties of the $Ge_{0.895}Fe_{0.105}$ films.

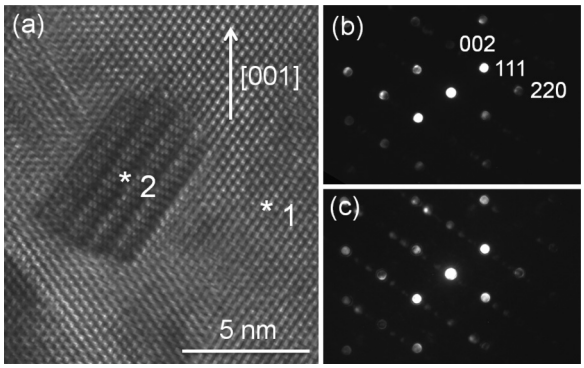

FIG. 2. (a) HRTEM lattice image projected along the Ge[110] axis of a ferromagnetic nanoparticle formed in the $Ge_{0.895}Fe_{0.105}$ film after annealing at 600 °C. (b) and (c) TED images taken in (b) the diamond-crystal-structure region (*1) and in (c) the nanoparticle (*2).

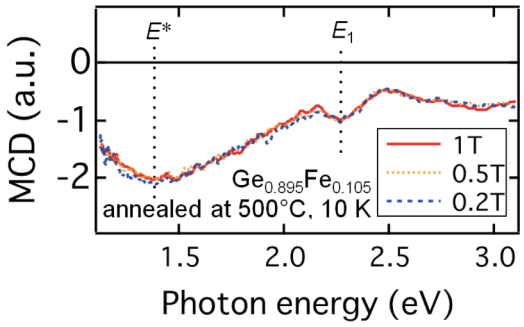

FIG. 3. (Color online) Normalized MCD spectra of the $Ge_{0.895}Fe_{0.105}$ film annealed at 500 °C with magnetic fields of 1 T (red solid curve), 0.5 T (orange dotted curve), and 0.2 T (blue broken curve) applied perpendicular to the film plane at 10 K.

Magnetic circular dichroism (MCD), which is defined by the difference between the optical reflectances of right- and left-circular polarized lights, is an effective tool to identify the origin of the ferromagnetism in the film. This is because the MCD intensity is enhanced at the critical-point energies of the band structure due to the spin splitting caused by the *s,p-d* exchange interactions, which are considered to be the origin of the ferromagnetism in FMSs [17], and because it is proportional to the vertical component of the magnetization *M*. Figure 3 shows the normalized MCD spectra of the $Ge_{0.895}Fe_{0.105}$ film annealed at 500 °C at different magnetic fields (0.2, 0.5, and 1 T) applied perpendicular to the film at 10 K. They are superimposed on a single spectrum over the whole photon energy range, indicating that the MCD spectrum originates from the nearly single ferromagnetic phase of GeFe [18] even though it has the nonuniform distribution of Fe atoms. As described later, although the nonuniformity induces weak spin-glass-like behavior in the very-low-temperature region, it is not strong enough to induce magnetic phase separation. This suggests that the locally high-Fe-concentration region and low-Fe-concentration region are magnetically coupled by the *s,p-d* exchange interaction, which results in the nearly homogeneous ferromagnetic behavior.

Figure 4(a) shows the MCD spectra of the Ge substrate, the as-grown $Ge_{0.895}Fe_{0.105}$ film, and the $Ge_{0.895}Fe_{0.105}$ film annealed at 400, 500, and 600 °C (from the top to the bottom) with a magnetic field of 1 T applied perpendicular to the film plane at 10 K. All the samples show the E_1 peak at around 2.3 eV corresponding to the *L* point of bulk Ge as we can see in the MCD spectrum of the Ge substrate and a broad peak (E^*) at around 1.4 eV. The E_1 peak enhanced by the *s,p-d* exchange interaction is a characteristic property of FMSs [19]. For the origin of the E^* peak, there are two possibilities; optical transitions from the impurity bands, which have been observed in III-V-based FMS $Ga_{1-x}Mn_xAs$ [20], and *d-d* transitions related to the crystal-field splitting of substitutional Fe atoms. The E_1 peak is suppressed by the annealing at 600 °C, which is thought to be related to the phase separation shown in Fig. 1(c). Generally, a MCD spectrum of a phase-separated material is expressed by the sum of these phases. During the annealing at 600 °C, the Fe atoms are removed from the region *1, and it becomes nearly pure Ge, which results in the decreased intensity of the E_1 peak. Figures 4(b)–4(d) shows the magnetic

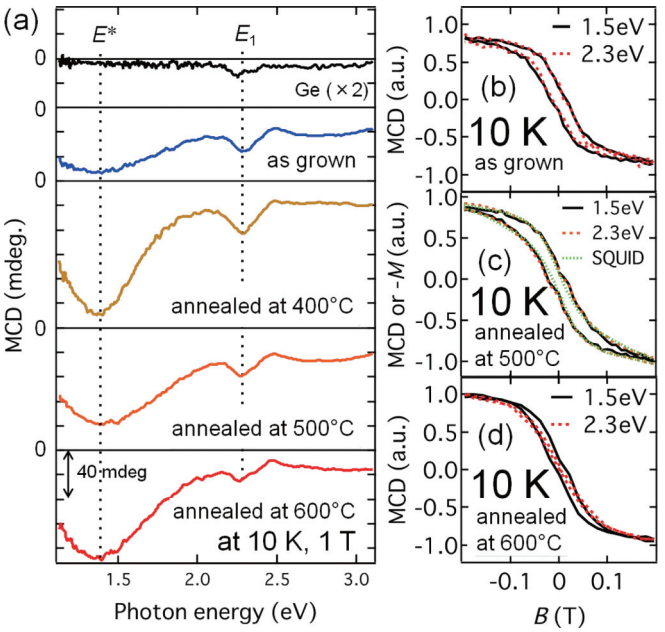

FIG. 4. (Color) (a) MCD spectra of the Ge substrate, the as-grown $Ge_{0.895}Fe_{0.105}$ film, and the $Ge_{0.895}Fe_{0.105}$ film annealed at 400, 500, and 600 °C (from the top to the bottom) with a magnetic field B of 1 T applied perpendicular to the film plane at 10 K. (b)–(d) Magnetic field dependence of the MCD at 1.5 eV (close to the E^* peak) and 2.3 eV (E_1 peak) for the GeFe films (b) as-grown and annealed at (c) 500 °C and (d) 600 °C. In (c), the green curve expresses the magnetic field dependence of the normalized -M measured by SQUID for the $Ge_{0.895}Fe_{0.105}$ film annealed at 500 °C.

field (B) dependence of the normalized MCD intensities at around E^* (1.5 eV, solid curve) and at E_1 (2.3 eV, dotted curve) for (b) the as-grown $Ge_{0.895}Fe_{0.105}$ film and for the $Ge_{0.895}Fe_{0.105}$ films annealed at (c) 500 °C and (d) 600 °C. Figure 4(c) also shows the B dependence of the normalized magnetization (M) for the $Ge_{0.895}Fe_{0.105}$ film annealed at 500 °C (green curve) measured by superconducting quantum interference device (SQUID). Here the diamagnetic signal of the Ge substrate was subtracted from the raw M data. In the as-grown GeFe film and the annealed film at 500 °C, the shapes of the curves at 1.5 and 2.3 eV are identical with each other, which means that the E^* and E_1 peaks originate from the nearly single ferromagnetic phase of GeFe as previously mentioned. Moreover, Fig. 4(c) shows that the hysteresis loops of MCD have the same shape as that of the M-B curve measured by SQUID at 10 K in the $Ge_{0.895}Fe_{0.105}$ film annealed at 500 °C. This indicates that the M data measured by SQUID has the same origin as that induces the spin splitting of the energy band of GeFe. Therefore we conclude that the origin of the magnetization is only the nearly single ferromagnetic phase of GeFe [21]. In contrast, after the annealing at 600 °C, the curves are not identical, which indicates that there are two or more magnetic phases in the film. These results mean that the GeFe layer was phase-separated magnetically and crystallographically by the annealing at 600 °C.

Figure 5(a) shows the magnetic field dependence of MCD at E_1(2.3 eV) of the $Ge_{0.895}Fe_{0.105}$ film annealed at 500 ºC measured at 10 K (blue curve), 150 K (green curve), 210 K

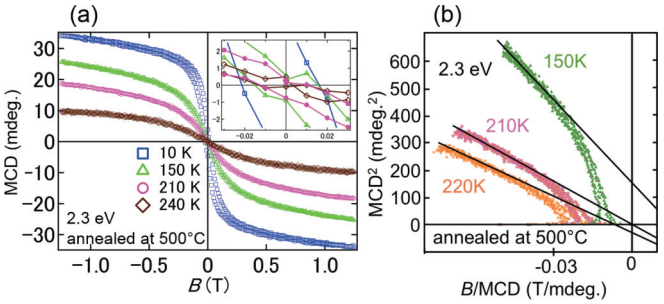

FIG. 5. (Color) (a) Magnetic field B dependence of the MCD intensity at E_1 (2.3 eV) of the $Ge_{0.895}Fe_{0.105}$ film annealed at 500 °C measured at 10 K (blue curve), 150 K (green curve), 210 K (pink curve), and 240 K (brown curve). The inset shows the close-up view near zero magnetic field. (b) Arrott plots of the MCD-B data at 2.3 eV measured at various temperatures for the $Ge_{0.895}Fe_{0.105}$ film annealed at 500 °C.

(pink curve), and 240 K (brown curve). The inset shows the close-up view near the zero magnetic field. A clear hysteresis curve is observed up to 210 K. We estimated the T_C values of our films by using the Arrott plots (MCD^2 – B/MCD), which were obtained from the MCD-B data. In the plots, we can estimate the square of the spontaneous MCD by extrapolating the data in the high magnetic field region. This method is well established and convenient because it is free from the effect of the magnetic anisotropy which affects the low magnetic field properties and sometimes makes the accurate estimation of T_C difficult. Figure 5(b) shows the Arrott plots of the MCD-B data at 2.3 eV for the $Ge_{0.895}Fe_{0.105}$ film annealed at 500 °C, indicating that the T_C is 210 K. The same T_C value is obtained both in the hysteresis loop analysis in Fig. 5(a) and the Arrott plots in Fig. 5(b).

Figure 6 shows the T_C of the $Ge_{0.895}Fe_{0.105}$ films estimated at the photon energy of 1.5 eV (square) and 2.3 eV (triangle). In the as-grown film, the T_C values at both of the photon energies are the same. When it is annealed at 400 or 500 °C, even though the film is magnetically homogeneous as discussed above, we see a slight difference in the T_C values between at 1.5 and 2.3 eV most likely due to the non-uniformity of the

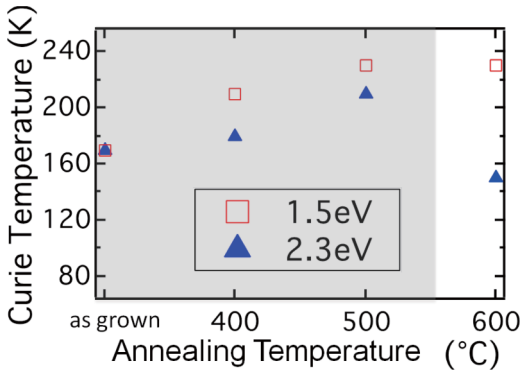

FIG. 6. (Color online) Curie temperature as a function of the annealing temperature of the $Ge_{0.895}Fe_{0.105}$ films estimated by the Arrott plot (MCD^2 – B/MCD) at the photon energies of 1.5 eV (square) and 2.3 eV (triangle).

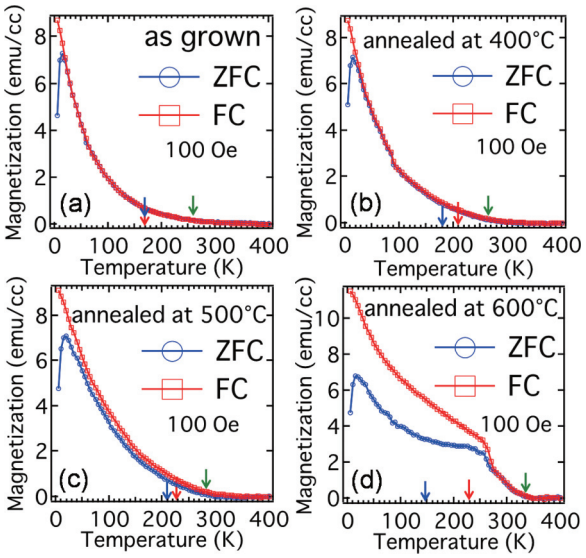

FIG. 7. (Color) Magnetization vs temperature (M-T) curves of the $Ge_{0.895}Fe_{0.105}$ samples (a) as-grown and annealed at (b) 400, (c) 500, and (d) 600 °C. The measurements were performed in the two processes of field cooling (FC, red curve) and zero-field cooling (ZFC, blue curve) with a magnetic field of 100 Oe applied perpendicular to the film plane. The red and blue arrows are the T_C values estimated by the Arrott plots of the MCD-B data obtained at 1.5 and 2.3 eV, respectively. The green arrows express θ_a estimated by the Curie-Weiss plots.

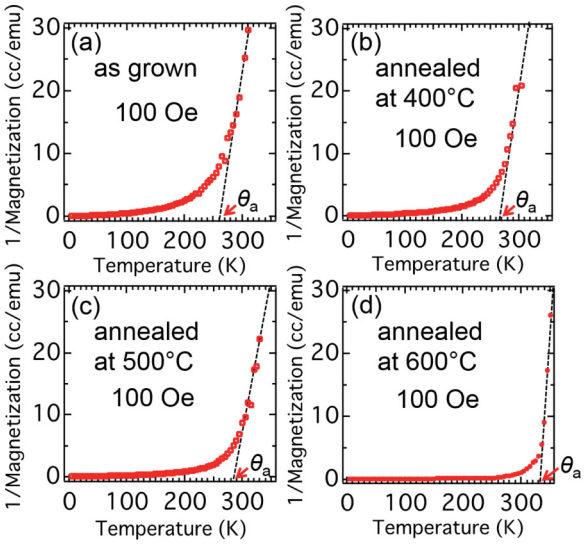

FIG. 8. (Color online) Inverse of M vs temperature ($1/M$-T) curves of the $Ge_{0.895}Fe_{0.105}$ samples (a) as-grown and annealed at (b) 400, (c) 500, and (d) 600 °C. The measurements were performed in the FC process.

Fe concentration, which is enhanced by the annealing. When the annealing temperature is 600 °C, the T_C values at 1.5 and 2.3 eV are completely different due to the phase separation.

The magnetization versus temperature ($M-T$) curves of the films were measured by SQUID. Figures 7(a)–7(d) show the $M-T$ curves of the $Ge_{0.895}Fe_{0.105}$ samples as grown and annealed at 400, 500, and 600 °C, respectively. In the zero-field-cooling (ZFC) process shown by the blue curves, M was measured with a magnetic field of 100 Oe applied perpendicular to the film plane with increasing temperature after the sample was cooled down to 5 K from room temperature without a magnetic field. In the field-cooling (FC) process shown by the red curves, M was measured with decreasing temperature from room temperature to 5 K under a magnetic field of 100 Oe applied perpendicular to the film plane. The red and blue arrows are the T_C values estimated by the Arrott plots obtained at 1.5 and 2.3 eV, respectively. The small leap of M at around 80 K in Fig. 7(b) is the artifact caused by the switching of the measurement range of SQUID. Figure 8 shows the Curie-Weiss plots ($1/M$-T curves) obtained in the FC process for the $Ge_{0.895}Fe_{0.105}$ films (a) as-grown and annealed at (b) 400, (c) 500, and (d) 600 °C. The high-temperature part is described by the Curie-Weiss law. The green arrows in Fig. 7 are the asymptotic Curie temperature θ_a deduced from these Curie-Weiss plots. The θ_a values are higher than the T_C values, which indicates the existence of the ferromagnetic domains above T_C in the GeFe films as mentioned below. The θ_a value is increased from 260 K (as-grown) to 285 K (annealed at 500 °C) by the annealing while the film keeps the single magnetic phase. This result means that the enhancement of the nonuniformity of the Fe concentration increases the ferromagnetic interaction in the locally high-Fe-concentration regions.

The M-T curves in Fig. 7 are characterized by the irreversibility between the ZFC and FC processes. In all the samples, a cusp is seen at around 15 K in the ZFC curves, being a characteristic feature of a magnetic random system like a spin glass. Similar phenomena were observed in III-V-based FMS GaMnAs [22], II-VI-based FMS ZnCrTe [23], and AuFe alloys [24]. In GaMnAs, this magnetic randomness comes from the difference of magnetic anisotropy between the low and high hole concentration regions [22], while it comes from existence of the antiferromagnetic interaction due to the RKKY interaction in AuFe alloys. In GeFe, it does not originate from the ferromagnetic intermetallic precipitates but from the nonuniform distribution of Fe atoms, which is observed by the EDX measurements. The position of the cusps is insensitive to the annealing temperature, indicating that the annealing does not much influence this weak spin-glass-like behavior. Here, the spin-glass transition temperature $T_{SG}(H)$, which is related to a typical scale of the anisotropy-energy barriers in the system, is defined as the temperature at which the difference between the M values in ZFC and FC processes appears when a magnetic field of H (Oe) is applied perpendicular to the film plane. When a material system is in a spin-glass-like phase, it is well known that $T_{SG}(H)$ follows the de Almeida-Thouless (AT) line [25] given by

$$T_{SG}(H) = T_{SG}(0)\left(1 - \alpha H^{\frac{2}{3}}\right), \quad (1)$$

where α is a constant. Figure 9 shows the H dependence of the $T_{SG}(H)$ of the as-grown $Ge_{0.895}Fe_{0.105}$ film with the AT line. In Fig. 9, we see that $T_{SG}(H)$ linearly decreases as $H^{2/3}$ increases, meaning that the weak spin-glass-like behavior appears in the very low temperature region at $T < T_{SG}(H)$ [26]. The extrapolation of the AT line back to $H = 0$ gives the spin glass transition temperature $T_{SG}(0)$ at zero magnetic field, which is estimated to be ~26 K in this case.

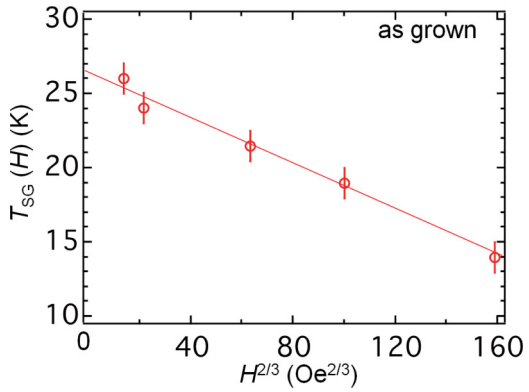

FIG. 9. (Color online) Magnetic field H dependence of the spin-glass transition temperature $T_{SG}(H)$ of the as-grown $Ge_{0.895}Fe_{0.105}$ film with the AT line.

Alternative-current susceptibility measurements may help more detailed understanding of it; however, it is difficult to measure it due to its small magnetic moment.

The notable point is that, when annealed at 600 °C, the sample shows another cusp at 260 K in the ZFC process shown in Fig. 7(d), which indicates the occurrence of phase separation and superparamagnetism. Moreover, the magnetic moment persists up to room temperature, indicating that the nano-particles, which have the high-Fe concentration with the periodic twins and stacking faults, have a high T_C value up to room temperature. These results obtained by SQUID show that the magnetic phase separation occurs at 600 °C, being consistent with the crystallographic and MCD analyses mentioned above.

V. DISCUSSION

In the case of the GeMn films, an α phase, which is very difficult to be distinguished from the host lattice only by the [110]-projection TEM image, has been observed in the GeMn nanocolumns [27,28]. In the case of our single-phase GeFe films, we can exclude the possibility of the existence of such nanocolumns because the surface of the GeFe films is very smooth with a small root-mean-square roughness r_{RMS} of 0.33 nm, which is comparable to that of the pure Ge film grown by LT-MBE [29], and we do not see any clear structures suggesting the existence of the nanocolumns on the surface. However, there might be a possibility that the α phase is embedded in the diamond crystal structure without any clear visible interface. We have carried out the channeling Rutherford backscattering (c-RBS) and c-particle-induced x-ray emission (c-PIXE) measurements [30], by which the Fe atoms in the α phase (if any) can be distinguished from the substitutional Fe atoms. In the $Ge_{0.935}Fe_{0.065}$ films grown at 160 and 240 °C, we have found that ~85% of the doped Fe atoms exist at the substitutional sites and ~15% of the doped Fe atoms exist at the interstitial sites. We have also clarified that T_C of GeFe is not correlated with the density of the Fe interstitials. Thus, even if the embedded α-phase exists in our films, it does not seem to be related to the ferromagnetism.

In the above sections, we have found that single-phase GeFe has the three critical temperatures; T_C, θ_a, and T_{SG} (0). From these three critical temperatures, we can infer the magnetic state in GeFe. Figure 10 shows the schematic diagrams of the magnetic states in the GeFe films after the sample was cooled down to 5 K from room temperature without a magnetic field and then temperature (T) is gradually increased with a magnetic field H (Oe) applied perpendicular to the film plane; (a1) $T_{SG}(H) > T$, (b) $T_C > T > T_{SG}(H)$, (c) $\theta_a > T > T_C$, (d) $T > \theta_a$, corresponding to the ZFC measurements. Figure 10(a2) shows the one after the sample was cooled down to T from room temperature with a magnetic field when $T_{SG}(H) > T$, corresponding to the FC measurements. Each small black arrow and big arrow represents the magnetic moment of each Fe atom and ferromagnetic domain, respectively. We note that, when $T > T_{SG}(H)$, the magnetic states in the ZFC and FC measurements are the same for the GeFe as-grown and annealed at 400 and 500 °C. In the high temperature region above θ_a, every Fe atom shows the paramagnetic behavior [Fig. 10(d)]. When $\theta_a > T > T_C$, the ferromagnetic domains that are formed by the short-range interaction appear in the locally high-Fe-concentration regions, resulting in the deviation from the Curie-Weiss law [Fig. 10(c)]. With decreasing T further, these ferromagnetic domains become larger, and the ferromagnetic transition of the whole system occurs at T_C [Fig. 10(b)]. Finally, the weak spin-glass-like behavior appears below $T_{SG}(H)$ [Figs. 10(a1) and 10(a2)]. We note that the hysteresis loops obtained in our single-phase films are not affected by this weak spin-glass-like behavior since this behavior is broken due to the initial magnetization process before the measurements.

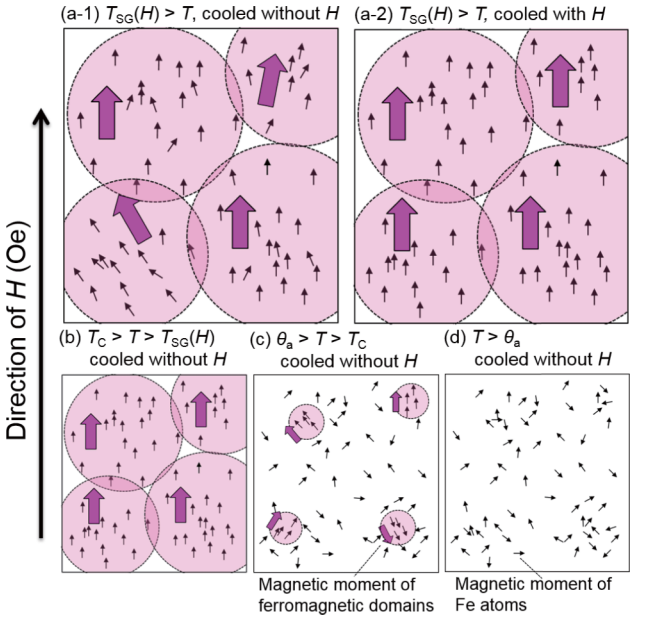

FIG. 10. (Color online) Schematic diagrams of the magnetic states in the GeFe films after the sample was cooled down to 5 K from room temperature without a magnetic field and then the temperature (T) is gradually increased with a magnetic field H (Oe) applied perpendicular to the film plane; (a1) $T_{SG}(H) > T$, (b) $T_C > T > T_{SG}(H)$, (c) $\theta_a > T > T_C$, (d) $T > \theta_a$, corresponding to the ZFC measurements, and (a2) the one after the sample was cooled down to T from room temperature with a magnetic field H when $T_{SG}(H) > T$, corresponding to the FC measurements.

The magnetic interaction in single-phase GeFe is complex because there is the magnetic randomness which comes from the nonuniform distribution of Fe atoms, resulting in the weak spin-glass-like behavior at very low temperature. However, the ferromagnetic interaction is obviously dominant because the T_C and θ_a values are much higher than T_{SG} and because more than half of M remains in the ZFC process even at 4 K. The origin of the ferromagnetic interaction is the *s,p-d* exchange interaction, which is confirmed by the enhancement of the E_1 peak in the MCD spectra [Fig. 4(a)]. The annealing enhances this ferromagnetic interaction, resulting in the increase in T_C and θ_a. Our results show that the increase in T_C is correlated with the enhancement of the nonuniformity of Fe atoms. In FMSs, such an increase in T_C with the enhancement of the nonuniformity of magnetic impurities is predicted theoretically [31,32]. Thus, to achieve room-temperature ferromagnetism, higher-Fe concentration and adequate enhancement of the nonuniformity of Fe atoms are needed.

In Fig. 5(a), the MCD-B curve at 240 K, which is above T_C(=210 K), has a large curvature, suggesting the existence of the superparamagnetism. This does not originate from the ferromagnetic intermetallic precipitates but from the ferromagnetic domains due to the nonuniform distribution of Fe atoms. This result also supports the model that the ferromagnetic interactions between the Fe atoms in the locally high-Fe-concentration regions are still remaining above T_C, as mentioned above.

The T_C values of the already-known equilibrium Fe-Ge compound phases are much higher than room temperature [33–35], which suggests that the ferromagnetic nanoparticles obtained by the annealing at 600 °C in this study are an unknown magnetic phase, which has a diamond crystal structure with periodic twins and stacking faults. The high T_C of the nanoparticles may originate from the high-Fe concentration, quantum confinement, or band structure modulation associated with the formation of twins [36]. The twin boundaries are viewed to be a regional wurtzite structure so these nanoparticles, which include periodic twin boundaries, may change their band structure and physical properties.

VI. SUMMARY

The annealing of the GeFe thin film in a nitrogen atmosphere was shown to be quite effective to enhance the ferromagnetism of GeFe. When the annealing temperature is lower than 600 °C, T_C is increased up to 210 K while the film keeps the nearly single FMS phase. When it is annealed at 600 °C, the ferromagnetic nanoparticles with a high T_C up to room temperature, which have a diamond crystal structure with twins and stacking faults, are formed in the GeFe film. We have clarified that the inhomogeneity of the Fe concentration plays an essential role in determining the ferromagnetism. The ferromagnetism is much stronger than the weak spin-glass-like behavior, that is caused by the nonuniform distribution of the Fe atoms, and it dominates the system. Both types of films have good compatibility with group IV (Ge and Si) semiconductor materials and devices, and thus they are very promising for realizing Si-based spin devices.

ACKNOWLEDGEMENTS

This work was partly supported by Giant-in-Aids for Scientific Research including Specially Promoted Research, Project for Developing Innovation Systems of MEXT, and FIRST program of JSPS. This work was partly conducted in Research Hub for Advanced Nano Characterization, The University of Tokyo, supported by the MEXT, Japan.

[1] Y. Wang, F. Xiu, Y. Wang, H. Xu, D. Li, X. Kou, K. L. Wang, A. P. Jacob, and Jin Zou, J. Cryst. Crowth **312**, 3034 (2010).
[2] Y. Shuto, M. Tanaka, and S. Sugahara, Jpn. J. Appl. Phys. **47**, 7108 (2008).
[3] Y. D. Park, A. T. Hanbibicki, S. C. Erwin, C. S. Hellberg, J. M. Sullivan, J. E. Mattson, T. F. Ambrose, S. Wilson, G. Spanos, and B. T. Jonker, Science **295**, 651 (2002).
[4] M. Jamet, A. Bsrski, T. Devillers, V. Poydenot, R. Dujardin, P. B. Guillemaud, J. Rothman, E. B. Amalric, A. Marty, J. Cibert, R. Mattana, and S. Tatarenko, Nat. Mater. **5**, 653 (2006).,
[5] Y. Jiang and Y. Wang, Adv. Mater. Sci. Eng. **2012**, 726921 (2012).
[6] S. Yada, P. N. Hai, S. Sugahara, and M. Tanaka, J. Appl. Phys. **110**, 073903 (2011).
[7] Y. Ban, Y. Wakabayashi, R. Akiyama, R. Nakane, and M. Tanaka, AIP Adv. **4**, 097108 (2014).
[8] Y. Shuto, M. Tanaka, and S. Sugahara, J. Appl. Phys. **99**, 08D516 (2006).
[9] Y. Shuto, M. Tanaka, and S. Sugahara, Phys. Status Solidi C **3**, 4110 (2006).
[10] Y. Shuto, M. Tanaka, and S. Sugahara, Appl. Phys. Lett. **90**, 132512 (2007).
[11] F. Xiu, Y. Wang, X. Kou, P. Upadhyaya, Y. Zhou, J. Zou, and K. L. Wang, J. Am. Chem. Soc. **132**, 11425 (2010).
[12] P. N. Hai, S. Ohya, and M. Tanaka, Nat. Nanotech. **5**, 593 (2010).
[13] P. N. Hai, S. Ohya, M. Tanaka, S. E. Barnes, and S. Maekawa, Nature **458**, 489 (2009).
[14] K. W. Edmonds, P. Bogusławski, K. Y. Wang, R. P. Campion, S. N. Novikov, N. R. S. Farley, B. L. Gallagher, C. T. Foxon, M. Sawicki, T. Dietl, M. Buongiorno Nardelli, and J. Bernholc, Phys. Rev. Lett. **92**, 037201 (2004).
[15] M. Malfait, J. Vanacken, V. V. Moshchalkov, W. Van Roy, and G. Borghs, Appl. Phys. Lett. **86**, 132501 (2005).
[16] T. J. Konno and R. Sinclair, Mater. Chem. Phys. **35**, 99 (1993).
[17] K. Ando, T. Hayashi, M. Tanaka, and A. Twardowski, J. Appl. Phys. **83**, 6548 (1998).
[18] H. Saito, V. Zayets, S. Yamagata, and K. Ando, Phys. Rev. Lett. **90**, 207202 (2003).
[19] K. Ando, H. Saito, V. Zayets, and M. C. Debnath, J. Phys.: Condens. Matter **16**, S5541 (2004).
[20] K. Ando, H. Saito, K. C. Agarwal, M. C. Debnath, and V. Zayets, Phys. Rev. Lett. **100**, 067204 (2008).
[21] H. Saito, V. Zayets, S. Yamagata, and K. Ando, Phys. Rev. B **66**, 081201 (2002).

[22] K. Hamaya, T. Watanabe, T. Taniyama, A.Oiwa, Y. Kitamoto, and Y. Yamazaki, Phys. Rev. B **74**, 045201 (2006).
[23] S. Kuroda, N. Ozaki, N. Nishizawa, T. Kumekawa, S. Marcet, and K. Takita, Sci. Technol. Adv. Mater. **6**, 558 (2005).
[24] V. Cannella and J. A. Mydosh, Phys. Rev. B **6**, 4220 (1972).
[25] J. R. L. de Almeida and D. J. Thouless, J. Phys. A **11**, 983 (1978)
[26] B. Martinez, X. Obradors, Ll. Balcells, A. Rouanet, and C. Monty, Phys. Rev. Lett. **80**, 181 (1998).
[27] S. Tardif, V. Favre-Nicolin, F. Lancon, E. Arras, M. Jamet, A. Barski, C. Porret, P. Bayle-Guillemaud, P. Pochet, T. Devillers, and M. Rovezzi, Phys. Rev. B **82**, 104101 (2010).
[28] E. Arras, F. Lancon, I. Slipukhina, E. Prestat, M. Rovezzi, S. Tardif, A. Titov, P. Bayle-Guillemaud, F. d'Acapito, A. Barski, V. Favre-Nicolin, M. Jamet, J. Cibert, and P. Pochet, Phys. Rev. B **85**, 115204 (2012).
[29] B. Shin, J. P. Leonard, J. W. McCamy, and M. J. Aziz, Appl. Phys. Lett. **87**, 181916 (2005).
[30] Y. K. Wakabayashi, S. Ohya, Y. Ban, and M. Tanaka, J. Appl. Phys. **116**, 173906 (2014).
[31] K. Sato, H. Katayama-Yoshida, and P. H. Dederichs, Jpn. J. Appl. Phys. **44**, L948 (2005).
[32] T. Fukushima, K. Sato, H. Katayama-Yoshida, and P. H. Dederichs, Phys. Status Solidi A **203**, 2751 (2006).
[33] K. Kanematsu, K. Yasukochi, and T. Ohoyama, J. Phys. Soc. Jpn. **18**, 920 (1963).
[34] E. Adelson and A. E. Austin, J. Phys. Chem. Solids **26**, 1795 (1965).
[35] K. Yasukochi and K. Kanematsu, J. Phys. Soc. Jpn. **16**, 429 (1961).
[36] D. P. DiVincenzo, O. L. Alerhand, M. Schlüter, and J. W. Wilkins, Phys. Rev. Lett. **56**, 1925 (1986).